Kent Academic Repository
Full text document (pdf)

Citation for published version

Zhang, Wenbiao and Yan, Yong and Qian, Xiangchen and Guan, Yanjun and Zhang, Kai (2016) Measurement of Charge Distributions in a Bubbling Fluidized Bed Using Wire-Mesh Electrostatic Sensors. IEEE Transactions on Instrumentation and Measurement . ISSN 0018-9456. (In press)

DOI

Link to record in KAR

http://kar.kent.ac.uk/59573/

Document Version

Author's Accepted Manuscript

Title: Measurement of Charge Distributions in a Bubbling Fluidized Bed Using Wire-Mesh Electrostatic Sensors

Author: Wenbiao Zhang [a]
Yong Yan [b], (Corresponding author)
Xiangchen Qian [a]
Yanjun Guan [c]
Kai Zhang [c]

Address: a) School of Control and Computer Engineering
North China Electric Power University
Beijing 102206, P.R. China
wbzhang@ncepu.edu.cn, xcqian@ncepu.edu.cn

b) School of Engineering and Digital Arts
University of Kent
Canterbury, Kent CT2 7NT, U.K.
y.yan@kent.ac.uk

c) Beijing Key Laboratory of Emission Surveillance and Control for Thermal Power Generation
North China Electric Power University
Beijing 102206, P.R. China
gyj0627@gmail.com, kzhang@ncepu.edu.cn

Abstract—In order to maintain safe and efficient operation of a fluidized bed, electrostatic charges in the bed should be monitored continuously. Electrostatic sensors with wire-mesh electrodes are introduced in this paper to measure the charge distribution in the cross section of the fluidized bed. A Finite Element Model is built to investigate the sensing characteristics of the wire-mesh sensors. In comparison with conventional electrostatic sensors, wire-mesh sensors have higher and more uniform sensitivity distribution. Based on the induced charges on the electrodes and the sensitivity distributions of the sensors, the charge distribution in the cross section of the fluidized bed is reconstructed. However, it is difficult to directly measure the induced charges on the electrodes. A charge calibration process is conducted to establish the relationship between the induced charge on the electrode and the electrostatic signal. Experimental studies of charge distribution measurement were conducted on a lab-scale bubbling fluidized bed. The electrostatic signals from the wire-mesh sensors in the dense phase and splash regions of the bed for different fluidization air flow rates were obtained. Based on the results obtained from the charge calibration process, the estimated induced charges on the electrodes are calculated from the Root Mean Square values of the electrostatic signals. The characteristics of the induced charges on the electrodes and the charge distribution in the cross section under different flow conditions are investigated, which proves that wire-mesh electrostatic sensors are able to measure the charge distribution in the bubbling fluidized bed.

Index Terms–wire-mesh electrostatic sensors; bubbling fluidized bed; charge distribution measurement; induced charge; Finite Element Modeling

I. INTRODUCTION

Bubbling fluidized beds, which have excellent heat and mass transfer efficiencies, are widely applied in chemical engineering, biomolecular engineering and food processing industries. Due to the contact and frictions between the particles and between the particles and wall, electrification is inevitable in a fluidized bed. The presence of electrostatic charges in the bed affects the operation of the bed. The hydrodynamics in the bed, such as bubble size and shape and solids mixing rate, changes with the level of electrostatic charges in the bed. If the charges on the particles exceed a critical value, the particles in the bed may adhere to the wall and even cause discharges and

explosion [1]. In order to maintain safe and efficient operation of the fluidized bed, the electrostatic charges and the flow dynamics of solid particles in the fluidized beds should be continuously monitored.

As an off-line measurement tool, Faraday cups were used to directly measure the charge density in the fluidized beds [2, 3]. However, charge generation and dispassion during the sampling process would influence the measurement result. Apart from Faraday cups, electrostatic probes were developed to measure the electrostatic charges in fluidized beds. A theoretical model was developed by Chen et al. to explain the electrical current signals due to the passage of isolated gas bubbles in a fluidized bed [5, 6]. Based on this model, a collision probe was built to measure the particle charge-to-mass ratios in a 2D bubbling fluidized bed. An induction probe, which was mounted flush with the outside wall of the fluidized bed, was also developed by Chen et al.. They applied a number of induction probes to measure the induced charge signals due to the passage of bubbles and the charge distribution around the bubbles was reconstructed with different algorithms [7-9]. He et al. [10, 11] developed a dual-tip electrostatic probe for the measurements of particle charge density and bubble properties in a bubbling fluidized bed. The estimated particle charge density and bubble rise velocity were in reasonable agreement with those obtained using a Faraday cup and video imaging. However, electrostatic probes can only provide localized charge distribution information near the electrode. In order to maintain an effective operation of the fluidized bed, the electrostatic charge distribution in the whole cross section of the bed should be monitored.

As a noninvasive tomography method, electrostatic tomography (EST) was applied to visualize the flow pattern and reconstruct the charge distribution in the pneumatic conveying pipeline [12-15]. A 16-electrode system was applied by Green et al. to reconstruct the concentration profile in a gravity conveyer [12]. Machida et al. combined a back projection algorithm with the least squares method to reconstruct the electrostatic charges carried by particles [13]. Zhou et al. used the permittivity distribution acquired from an electrical capacitance tomography (ECT) system to improve the charge sensitivity field of an EST system and to reduce the uncertainty relating to the charge distribution reconstruction [14]. However, the sensitivity distribution of the sensor used for the EST system is not uniform, which may result in reconstruction errors, especially in the central area of the pipe. In addition, as charges stay on particle surface, the EST method requires the

information of the size and the shape of the particles to reconstruct the solids concentration profile.

In order to overcome the above drawbacks in the charge distribution measurement, wire-mesh electrostatic sensors are introduced in this paper. In comparison with ring-shaped and arc-shaped electrodes, the wire-mesh electrodes have higher and more uniform spatial sensitivity especially in a large diameter fluidized bed. The drawback of the electrodes is that the wire-mesh can obstruct the flow of particles and hence suffer from wear problems. However, the degree of obstruction depends on the diameter of the wire and the spacing between them and a wear resistant material can be used to prevent the abrasion of the wire. A detailed comparison of the existing methods for particle charge measurement is summarized in Table 1.

Table 1: Comparison of the existing methods for particle charge measurement

Methods	Sampling requirement	Intrusiveness	Sensitivity distribution	Measurement results
Faraday cups	Sampling of particles is required, charge generation and dispassion during the process may influence the result.	Intrusive	Sensitivity to the particles inside the cup	Electrostatic charge on the samples
Intrusive probes	Not required	Intrusive and the blockage depends on the size and the number of the electrodes	Only sensitive to the particles near the probes	Charge on the particles near the probe
Electrostatic tomography	Not required	Non-intrusive	Sensitivity distribution is not uniform, especially in the central area of the pipe	Reconstructed charge distribution may not represent the true distribution due to non-uniform sensitivity.
Wire-mesh electrostatic sensors	Not required	Intrusive and the blockage depends on the size and the number of the electrodes	Higher and more uniform sensitivity distribution	Cross-sectional charge distribution

Wire-mesh sensors have already been widely applied in the measurement of gas-liquid and liquid-liquid two-phase flows based on the capacitive and conductive methods. Pena and Rodriguez presented a review of the applications of wire-mesh sensors to multiphase flow measurement [16]. The advantages and disadvantages of wire-mesh sensors were analyzed.

Wire-mesh electrostatic sensors were applied to measure the size of pneumatically conveyed particles [17], with the relative error of the mass median particle size being no greater than 15%. Preliminary results of the charge distribution reconstruction in a gravity drop test rig were reported at the IEEE International Instrumentation Measurement Technology Conference in 2016 [18]. It is proved that the charge distribution can be reconstructed using the induced charges on the electrodes and the sensitivity distributions of the sensors, which needs further verification in the real experimental set-up. This paper presents more detailed experimental results along with interpretations of charge distribution measurement using wire-mesh electrostatic sensors. Since it is difficult to directly measure the induced charges on the electrodes, a charge calibration process is conducted to establish the relationship between the induced charge on the electrode and the electrostatic signal from the wire-mesh sensors. The estimated induced charges on the electrodes of the wire-mesh sensors are applied to reconstruct the charge distributions in the dense phase and splash regions of the bubbling fluidized bed.

II. SENSOR DESIGN AND FEM MODELLING

A. Sensor design

In a bubbling fluidized bed, with the movement of bubbles, electrostatic charges are generated due to the interactions between particles, the frictions between particles and walls of the fluidized bed and the relative motion of the particles with air. In this study wire-mesh electrostatic sensors are applied to measure the charge distributions in different parts of a bubbling fluidized bed. The sensors and their installation on the fluidized bed are shown in Figure 1.
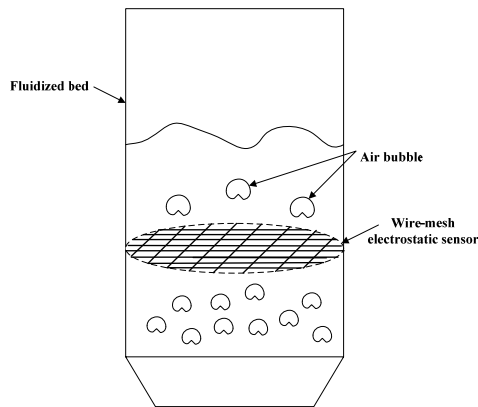

Figure 1 Wire-mesh electrostatic sensors on a bubbling fluidized bed

The electrodes of wire mesh electrostatic sensors are made up from two mutually perpendicular

strands of insulated wires with a diameter of 1.5 mm. In view of the inner diameter of the fluidized bed (180 mm) and in order to improve the spatial resolution of the charge distribution measurement, a set of 8 parallel wires with an even spacing of 20 mm in each strand are used to encompass the cross section. A thin wire will have less obstruction to the flow, but it is prone to break under the intensive contact and frictions by the dense particles flowing in the bubbling bed. By taking the strength of the wires and the obstruction to the particulate flow into account, the wires are made from stainless steel with a diameter of 1 mm. Shrinkable plastic tubes, with a thickness of 0.25 mm, are fitted outside the wires to prevent the direct charge transfer between the charged particles and the wires. When the charged particles pass through the mesh, charges are induced on different electrodes of the sensors. By measuring the induced charges from the electrodes, the charge distribution in the cross section of the fluidized bed is reconstructed. In the present sensor design, approximately 14% of the cross section is blocked by the wires. With relatively less number of wires and larger spacing between them, the effect of the blockage by the wires is reduced. With the continuous charging of solid particles, the accumulation of charges on the particles will introduce electric discharge in the bubbling bed and the discharge results in the spikes in the signal. However, this effect is minimized in the signal conditioning electronics of the measurement system. Figure 2 shows a photo of the wire-mesh electrostatic sensors. With the fluctuation of electrostatic charges on the particles and their movement, a minute change in electric current is detected on the electrode. The current signal is converted to a voltage signal through a pre-amplifier. By taking the spatial filtering effect into account, the bandwidth B of the electrostatic signal can be estimated according to the following equation:

$$B = K_b \frac{V_m}{W}$$

(1)

where V_m is the mean velocity of particles, W is the axial width of the electrode and K_b is a proportionality coefficient and estimated to be below 0.3 according to reference [19]. Since the mean velocity of particles is usually less than 1 m/s in the bed and the axial width of the electrode is 1.5 mm, the bandwidth of the electrostatic signal is thus estimated to be below 200 Hz. As a result, the signal is fed into a second-order low-pass filter with a bandwidth of 1000 Hz, which is enough for the dynamics response of the measurement system. Finally, the signal is further amplified through a gain adjustable amplifier. The schematic diagram of the signal conditioning circuit is available in reference [20]. The electrostatic signals from all electrodes were sampled

6

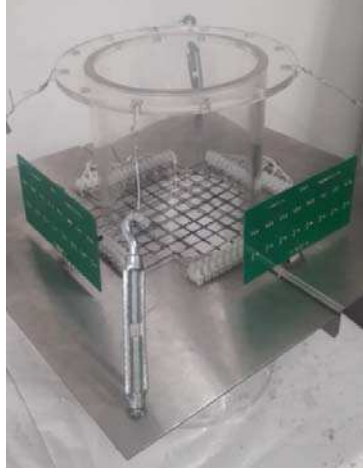simultaneously with a sampling frequency of 2 kHz.

Figure 2 Wire-mesh electrostatic sensors

B. FEM modeling of the sensors

In order to improve the performance of the wire-mesh electrostatic sensors, the sensing characteristics of the sensors are analyzed. The electrostatic field due to the charged particles in the fluidized bed is governed by the following equation:

$$\nabla^2 \varphi = -\frac{\rho}{\varepsilon_0 \varepsilon_r} \tag{2}$$

where φ is the electrical potential, ε_0 is the permittivity of free space, ε_r is the relative permittivity of the material and ρ is the charge density in the fluidized bed. After solving the electrical potential, the surface charge density σ is found from the relation:

$$\sigma = \varepsilon_0 \varepsilon_r E = -\varepsilon_0 \varepsilon_r \nabla \varphi \tag{3}$$

The quantity of induced charge q_i on the surface of the wire is calculated from:

$$q_i = \int_s \sigma ds \tag{4}$$

In view of the wire-mesh structure of the electrostatic sensors (Figure 2), it is impossible to find an analytical solution to the above equations. However, it is possible to build a Finite Element Method (FEM) model to analyze the characteristics of the sensors. An FEM model of the wire-mesh electrostatic sensors is built using COMSOL, as shown in Figure 3. A cylinder with the same diameter of the fluidized bed (180 mm) is set to be the model domain. A set of 16 cylinders with a diameter of 1.5 mm is used to model the wire-mesh. The permittivity of the material and the thickness of the insulation layer will affect the capacitance between the charged particles and the electrode, which will further affect the induced charge on the electrode. Since the thickness of

7

the insulation layer in the real system is only 0.25 mm, it has less effect on the sensing characteristics of the wire-mesh electrodes. As a result, the effect of the insulated material is not considered in the FEM modeling. A sphere with a radius of 1 mm is applied to model the charged particle. The materials of the wires and the model domain are set to steel and air respectively. The relative permittivity of the particle is set to 2.5 and the charge on the particle is set to 1 μC. The boundary condition is set to ground for the electrodes and zero charge for the outer surface of the model domain. Tetrahedral quadratic Lagrange elements are used in the mesh mode of the FEM model. The wire electrodes are meshed much finer than other subdomains so as to reflect the charge distribution in the electrode explicitly. In order to obtain the sensitivity distribution of the sensor, the cross section is divided into a 9 × 9 grid. During the simulation, the charged particle is placed in the center of different grids of the cross section and the induced charge on each electrode of the sensors are calculated according to equations (2)-(4).
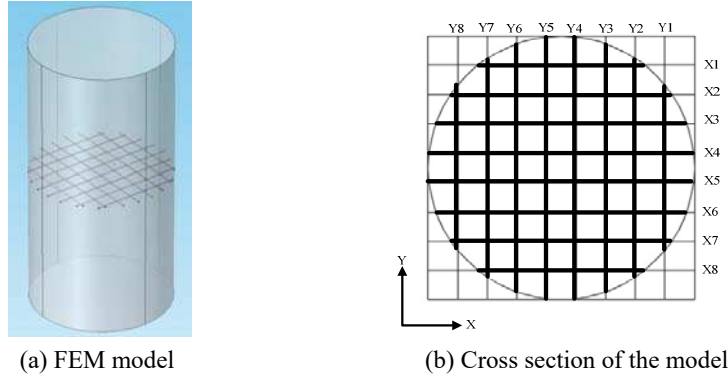

(a) FEM model (b) Cross section of the model

Figure 3 Finite element modeling of the wire-mesh electrostatic sensors

The sensitivity $S_i (x, y)$ of the ith electrode of the wire-mesh sensors when the charged particle is placed in the position (x, y) of the cross section is calculated by

$$S_i(x, y) = \frac{q_i}{q_s} \tag{5}$$

where q_i is the induced charge on the ith electrode and q_s is the charge on the particle. By placing the charged particle in different positions of the cross section, the sensitivity profile of each electrode of the sensor is obtained. The sensitivity distribution of the wire-mesh sensors is shown in Figure 4. It can be concluded from the sensitivity profiles of electrodes X1 and X4 that each electrode is more sensitive to the charged particle near the wire. The sensitivity distribution $S(e)$ of the whole sensors is obtained by summing up the sensitivity profiles of all the electrodes, as

8

shown in Figure 4 (c).

$$S(e) = \sum_i S_i(e)$$

(6)

where e is the element in the cross section where the sensitivity is not zero. The average sensitivity of the sensor is 0.985 and the relative deviation of the sensitivity at each point from the average value is shown in Figure 4 (d), which is less than ±0.2 %. As shown in Figure 6 of reference [21], it is found that the arc-shape electrode is only sensitive to the charged particles near the electrode and the sensitivity in the center of the ring-shape electrode is much lower than that of the region near the electrode. It is evident that the wire-mesh sensors have a higher and more uniform sensitivity distribution than other forms of electrostatic sensors.
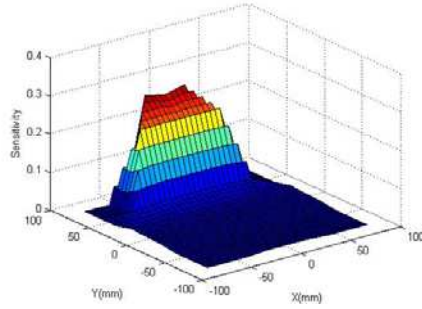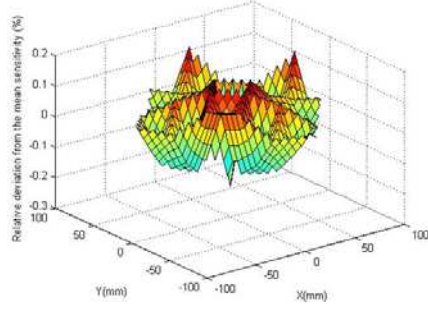

(a) Sensitivity distribution of electrode X1
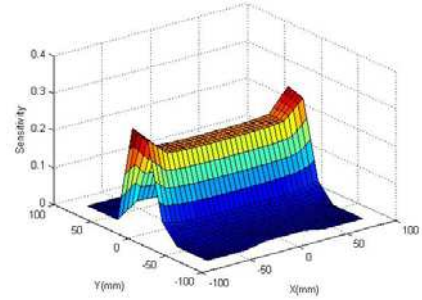
(b) Sensitivity distribution of electrode X4
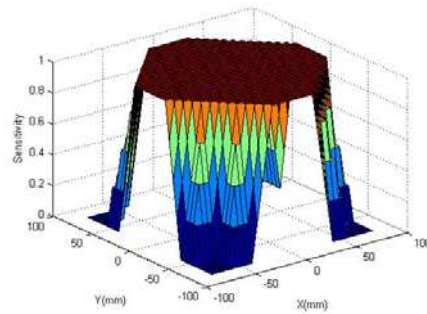
(c) Sensitivity distribution of the whole sensor

9

(d) Relative deviation from the mean sensitivity

Figure 4 Sensitivity distribution of the wire-mesh electrostatic sensors

C. Optimization of electrode structures

In order to optimize the matrix size and the spacing between the wires, FEM Models are applied to investigate the homogeneity of the sensitivity distribution of different number of electrodes. Based on the inner diameter of the bed (180 mm), the wire-mesh of 4×4, 6×6 and 8×8 electrodes are considered and the corresponding distances between the wires are 36 mm, 26 mm and 20 mm, respectively. According to the process given in Section II. B, the sensitivity distributions for different numbers of electrodes are obtained. The homogeneity of the sensitivity distribution is calculated according to the following equation:

$$S^{avg} = \frac{1}{n}\sum_{e=1}^{n}S(e)$$

$$S^{dev} = \frac{1}{n-1}\sum_{e=1}^{n}(S(e)-S^{avg}(e))$$

$$H = \frac{S^{dev}}{S^{avg}} \times 100\%$$

(7)

where S^{avg} and S^{dev} are the average and the standard deviation of the sensitivity distribution. H is the homogeneity of the sensitivity distribution. The smaller the H, the more homogeneous the sensitivity distribution. The homogeneity of the sensitivity distribution for different numbers of electrodes is given in Figure 5. It is found that the sensitivity distribution of 8×8 electrodes is more homogenous than the wire-mesh of 4×4 and 6×6 electrodes. Meanwhile, the blockage of the wire-mesh sensors for different numbers of the electrodes is also given in Figure 5. With more electrodes such as 10×10, the degree of obstruction is higher. Considering a trade-off between the homogeneity of the sensitivity distribution and the obstruction by the electrodes, we regard the wire-mesh of 8×8 electrodes as the optimum and thus have applied in the present study.
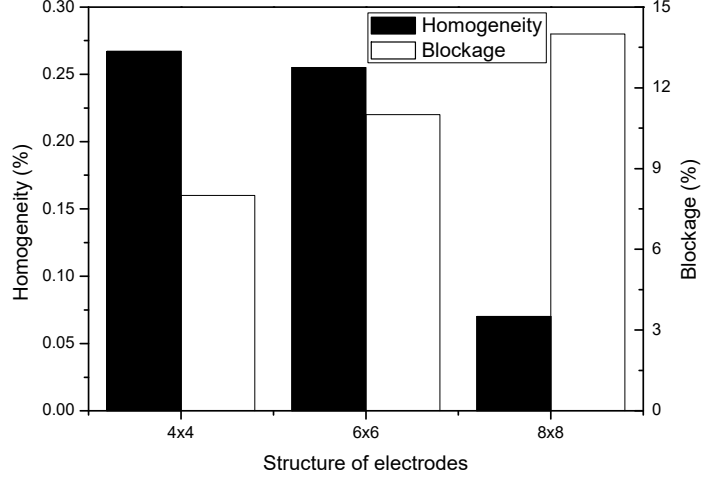
10

Figure 5 Homogeneity of the sensitivity distribution and the blockage of the wire-mesh sensors for different numbers of electrodes

III. PRINCIPLE OF CHARGE DISTRIBUTION MEASUREMENT

A. Charge distribution measurement

Given the sensitivity distributions of the wire-mesh sensors, if the charge distribution in the fluidized bed is known, the induced charge on each electrode is calculated. Inversely, if the induced charge on each electrode is available, the charge distribution in the cross section can be reconstructed. The charge distribution reconstruction method is explained by the following equation:

$$q_{rec}(x, y) = \frac{1}{16} \sum_{i=1}^{16} \frac{q_i}{S_i(x, y)} \tag{8}$$

where $q_{rec}(x, y)$ is the reconstructed charge in the position (x, y), q_i is the induced charge on the ith electrode of the sensors and $S_i(x, y)$ is the sensitivity of the ith electrode in the position (x, y). According to equation (4), the charge on particle q_s in the position (x, y) is obtained by dividing the induced charge q_i on the ith electrode with the sensitivity $S_i(x, y)$ of the ith electrode. The reconstructed charge in the position (x, y) is the average of the contributions from all the electrodes of the sensor. By calculating the reconstructed charge in different positions of the cross section, a 9×9 matrix of the charge distribution is obtained. Finally, the reconstructed charge distribution is calculated by the triangle-based linear interpolation from the 9×9 matrix. In order to validate the method of charge distribution reconstruction, numerical simulations using the FEM model mentioned in Section II are conducted. A charged spherical particle with a diameter of 2 mm and surface charge of 1 μC is placed in the center of the wire-mesh sensors. By using the

11

FEM model, the induced charge on each electrode is calculated. According to equation (6), the reconstructed charge distribution is obtained and shown in Figure 6. Since the induced charge on the electrode has opposite polarity from that on the particle, the peak value of the reconstructed charge distribution is -0.999 µC, which is very close to the charge on the particle. As a result, the proposed reconstruction method can be used to obtain the charge distribution of solid particles in the fluidized bed.
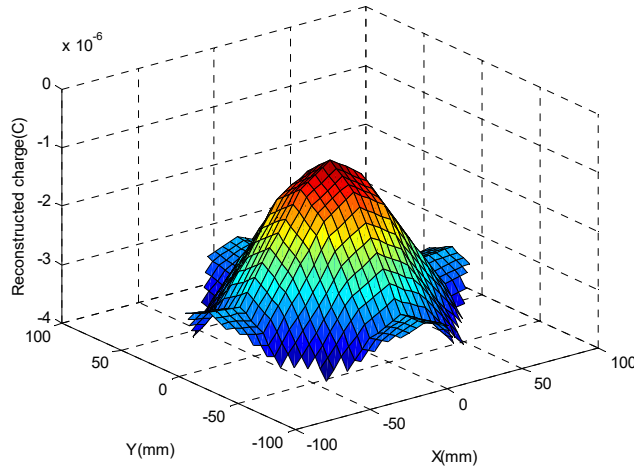

Figure 6 Reconstructed charge distribution due to a charged particle in the center of the wire-mesh sensors

B. Charge calibration process

According to equation (5), the induced charge on each electrode of the sensors should be measured in order to reconstruct the charge distribution. However, it is difficult to directly measure the induced charge on each electrode of the wire-mesh electrostatic sensors. The electrostatic signal is generated due to the fluctuation of induced charge on the electrode, which is related to the charges on the particles in the sensitivity volume of the electrode. In order to measure the charge distribution of solid particles in the fluidized bed, a charge calibration process was conducted to establish the relationship between the induced charges and the electrostatic signals generated from the sensors. However, due to the complexity associated with tribo-charging of solid particles in the fluidized bed, it is difficult to control and measure the charges on the particles during the experiments [22-24]. In the present study, a capacitor with time varying charge was used to generate the electrostatic signals on the wire-mesh sensors. Charge Q on the capacitor is proportional to the voltage V across the capacitor ($Q=CV$, where C is the value of the capacitance).

12

The experimental set-up of the charge calibration process is shown in Figure 7. In consideration of the advantages of compactness and high stability, a polypropylene film capacitor (100 nF with ±5% tolerance) was selected. During the experiments the capacitor was placed in the center of the wire-mesh sensors and charged with a sinusoidal voltage signal via a signal generator (Tektronix AFG3021B). The sinusoidal voltage on the capacitor generated a time-varying electrostatic field and hence induced charges on the electrodes. In this method the small capacitor acts as a charged particle and the charge on the capacitor is adjustable. In order to minimize the influence of the low frequency noise, the frequency of the sinusoidal voltage signal was set to 500 Hz. The electrostatic signal from each electrode of the wire-mesh sensors is obtained from the signal conditioning circuit (Section II). In the signal processing stage, a Chebyshev-type band-pass filter was applied to remove the low frequency noise. The cut-off frequencies of the band-pass filter are 475 Hz and 525 Hz, respectively, with stop-band attenuation 60 dB. The Root Mean Square (RMS) magnitude of the electrostatic signal is an indication of the signal fluctuation and thus RMS value of the filtered signal is calculated to reflect the quantity of the induced charge on the electrode. In addition, the induced charge on each electrode of the sensors is estimated from the charge on the capacitor and the sensitivity distribution of the electrode, which is obtained from the FEM modeling. As a result, the ratio between the induced charge on each electrode and the RMS value of the signal is obtained. This ratio is used to estimate the induced charge from the electrostatic signal.
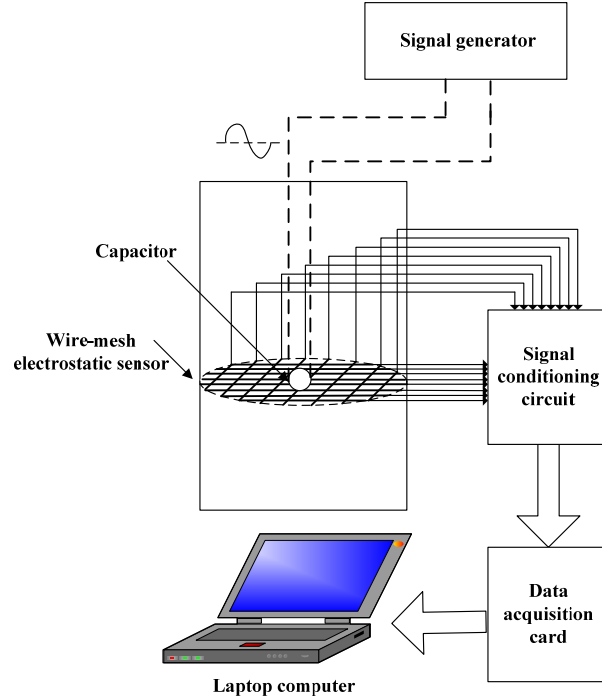
Figure 7 Experimental set-up of the charge calibration process
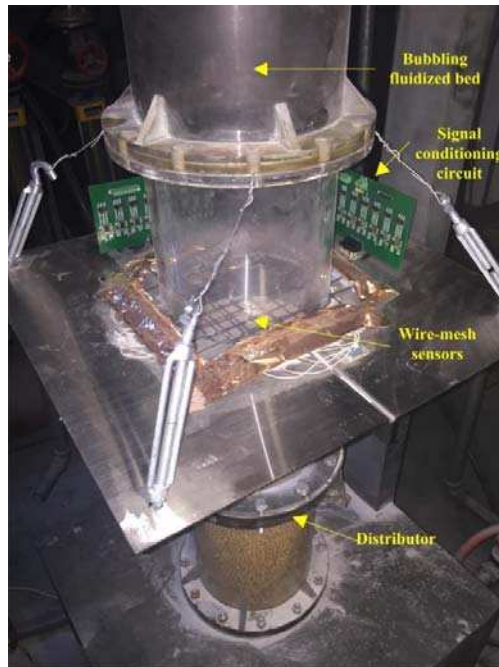
IV. EXPERIMENTAL SETUP

Based on the flow dynamics of solid particles in a bubbling fluidized bed, the flow regions can be categorized as dense phase region, splash region and freeboard region. Dense phase region is the region below the static bed height, while splash region is between the static bed height and the expanded bed height. The experimental analyze in present work can be divided into two groups, which are the charge distribution measurement in the dense phase region and the splash region of the bubbling fluidized bed respectively. The layout of the bubbling fluidized bed and the distribution of wire-mesh sensors are shown in Figure 8 (a) and a photo of the experimental set-up is given in Figure 8 (b). The fluidized bed was made of transparent Plexiglas with an inner diameter of 180 mm and a height of 2000 mm. A perforated-plate distributor (with a pore diameter of 1.5 mm and an open area ratio of 2.6%) was fitted at the bottom of the fluidized bed. The wire-mesh electrostatic sensors were installed at the position of 250 mm above the distributor. During the experiments sand particles were fluidized by air from a blower. The temperature and relative humidity of the air before entering the fluidized bed were $18^{\circ}C$ and 27%, respectively. The variations in environmental factors, such as the temperature and relative humidity of fluidization air, will affect the charge distribution in the bubbling fluidized bed and hence the output of the

14

measurement system. For example, the charges on the particles will decrease with the increase of relative humidity. The moisture content of the fluidizing air does not change the rate of charge generation, but increases the rate of charge dissipation. It is found in some studies that high relative humidity helps reducing electrostatic charges and reactor wall fouling in the bed [25, 26]. On the other hand, excessive humidification (>70%) is found to result in an instable bed that is difficult to fluidize due to capillary forces [27]. As a result, the expected range of humidity for the present measurement system to work is below 70%. The relative permittivity of the sand particles is 2.5 and the true density of the particles is 2500 kg/m^3. The particle size ranged from 150 μm to 200 μm, which was obtained from the vibratory sieve shaker AS 200 (Retsch, Germany), whilst the shape of the particles is roughly spherical. The particles were dried before each test run to eliminate humidity effects. The minimum fluidization velocity was obtained from the conventional pressure drop method [28], which was 0.013 m/s for present sand particles. The fluidization air flow rate is varied from 2.4 m^3/h to 12 m^3/h during the experiments, which was measured using a rotameter. The air flow rate ranged from two to ten times of minimum fluidization air flow rate under present experimental set-up and the bubbling and turbulent flow patterns can be observed in the fluidized bed. At the beginning of the experiments, particles were charged to a saturate level after fluidization for a long time (over 20 minutes). After that, by using the wire-mesh electrostatic sensors and the corresponding signal processing and acquisition system, the electrostatic signals for different fluidization air flow rates in the dense phase and the splash regions of the bubbling fluidized bed were obtained. Based on the algorithm of charge distribution reconstruction and the ratio between the induced charge on the electrode and the electrostatic signal, which is obtained from the charge calibration process, the characteristics of the charge distribution in different parts of the fluidized bed were investigated.
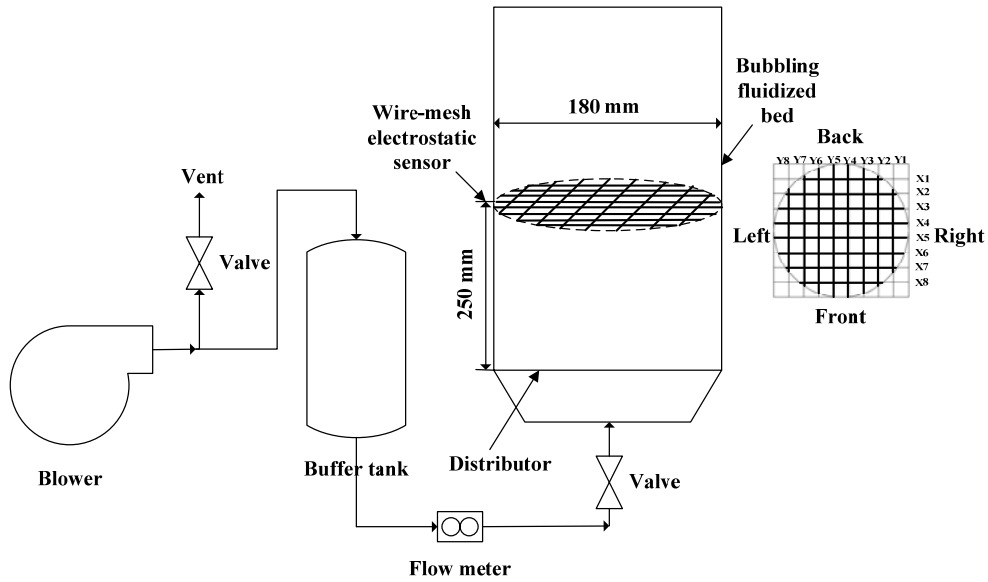
(a) Layout of the experimental set-up

(b) Photo of the bubbling fluidized bed and the wire-mesh sensor

Figure 8 Experimental set-up

V.   RESULTS AND DISCUSSION

A.   Dense phase region

During the experiments conducted in the dense phase region of the bed, the solid particles were initially added, forming a static bed height of 345 mm. Since the wire-mesh sensors are installed at the position of 250 mm above the distributor, the electrostatic signals from the sensors represent the characteristics of the charge distribution in the dense phase region. Solid particles in the dense

phase region move mainly upwards and the solids concentration is high. A typical electrostatic signal from sensors is shown in Figure 9 (a). With the electrical discharge of the charges on the particles, the spikes are generated in the electrostatic signal. Although this effect is minimized in the signal conditioning electronics, there are still some spikes present in the signal, as shown in Figure 9 (a), and they will affect the RMS value of the signal. As a result, a signal filtering process was conducted using the Wavelet Toolbox of MATLAB. The filtering of the signal was accomplished through wavelet denoising where Daubechies wavelet of order four was selected. Since the useful component of the electrostatic signal was below 200 Hz and the sampling frequency was 2000 Hz, three-level frequency components were decomposed. Besides, soft thresholding method was used to filter the spikes and the noise in the original signal. The signal after the wavelet denoising is plotted in Figure 9 (b). It is found that the spikes and the noise are removed from the electrostatic signal.

(a) Original signal   (b) Filtered signal
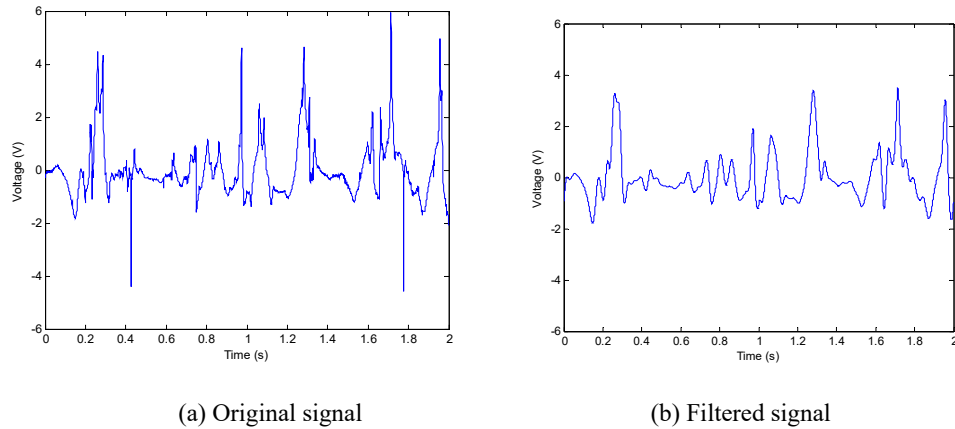Figure 9 A typical electrostatic signal from the wire-mesh electrostatic sensors

RMS values of the filtered signals from different electrodes for different air flow rates are calculated. In the calculation process, each RMS value is calculated from 4000 data of the signal. Based on the ratio from charge calibration experiments, induced charges on different electrodes of the wire-mesh sensors are calculated from the RMS values of the electrostatic signals. Induced charges on electrodes X1 and X4 for fluidization air flow rates of 2.4 m^3/h and 7 m^3/h are shown in Figure 10. With the fluctuation of solids concentration and solids velocity in the dense phase region, there are large variations of charges on particles and thus the induced charges on the wire-mesh sensors fluctuate during the sampling period. The average induced charge on electrode X4 is higher than that on electrode X1 under the same fluidization air flow rate and the offset is

17

caused by the difference of solids velocity between the center and the wall of the bed.

(a) Fluidization air flow rate 2.4 m³/h　　(b) Fluidization air flow rate 7 m³/h
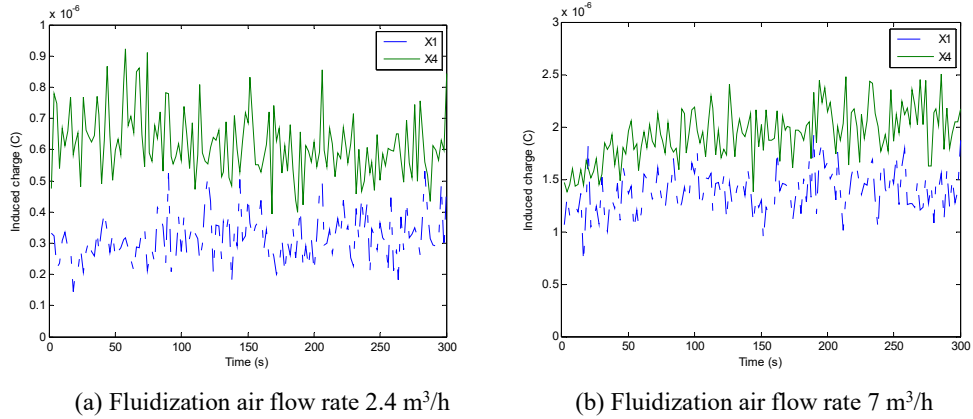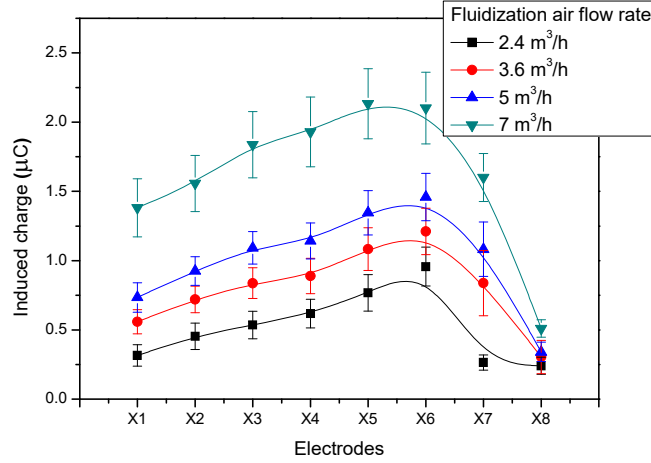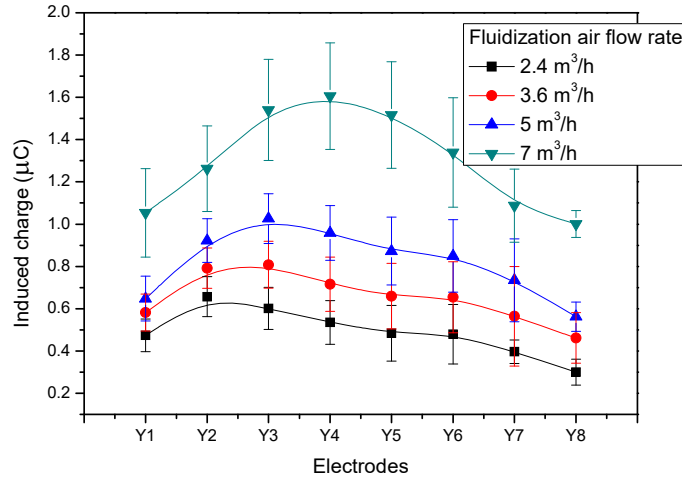
Figure 10 Induced charges on electrodes X1 and X4 in the dense phase region

The sampling duration of the electrostatic signal is 300 seconds and the induced charge on the electrode is calculated every two seconds, thus 150 induced charges are obtained. Time averaged and corresponding standard deviations of induced charges on different electrodes at different fluidization air flow rates in the dense phase region are given in Figure 11. The average induced charge on the electrode in the center of the cross section is higher than that on the electrode near the wall, which is the same as the results in Figure 10. Besides, the average induced charges on all electrodes increase with the fluidization air flow rate. In the dense phase region, the particles in the near wall region have a lower velocity than that in the center due to the wall effect of the bed. Meanwhile, the particles in the near wall region may move downwards. Due to the difference in the solids velocity between the center and the near wall region, the electrostatic charges on the particles depend on radial positions. As a result, the induced charge on the electrode in the center of the cross section is higher. The rising velocity of the bubbles increases with the fluidization air flow rate and the flow of the particles becomes more turbulent. Thus, charges on the particles increase due to the higher possibility of tribo-charging and the induced charges on all electrodes increase. In addition, the difference in solids velocity between the center and the near wall region increases with the fluidization air flow rate and the difference in the induced charge between the electrode in the center and that near the wall increases. Figure 11 shows that the standard deviation of the induced charge on electrode X4 is higher than that on electrode X1. In addition, the standard deviations of induced charges on electrodes X1 and X4 increase with the fluidization air flow rate. The reason for the above results is that, in the bubbling fluidized bed, the flow dynamics in the center of the bed is more turbulent than that near the wall and thus the fluctuation of the induced

charge on electrode X4 is higher. Besides, the flow behavior of solid particles becomes more turbulent with the increase of fluidization air flow rate, leading to increased fluctuation in the induced charge.

(a) Electrodes X1 to X8

(b) Electrodes Y1 to Y8

Figure 11 Time averaged and corresponding standard deviations of induced charges on different electrodes in the dense phase region

Charge distribution in the dense phase region can be reconstructed using the average induced charges on the electrodes according to equation (8). Figure 12 shows the reconstructed charge distribution in the cross section for fluidization air flow rate of 7 m^3/h. The color bar represents the estimated quantity of the charge. Although the charges in the center of the cross section are higher, the charge distribution in the cross section of the dense phase region is relatively uniform. However, it can be found that the charges in the back wall region are lower because of the non-uniform air flow distribution due to the air distributor under the bed.
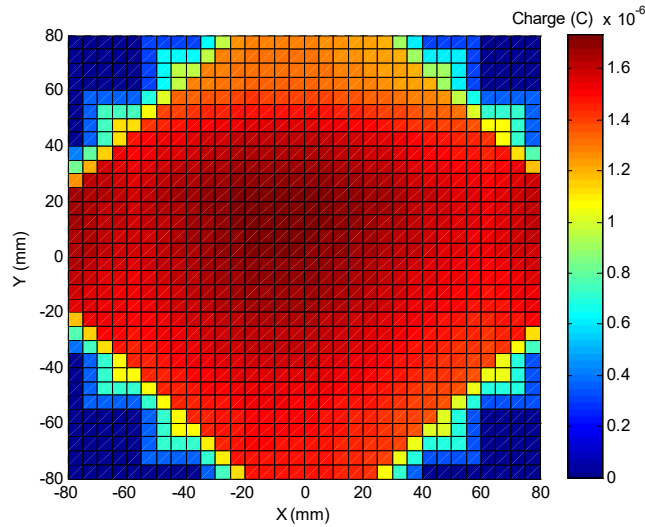
Figure 12 Reconstructed charge distribution in the dense phase region for fluidization air flow rate of 7 m³/h
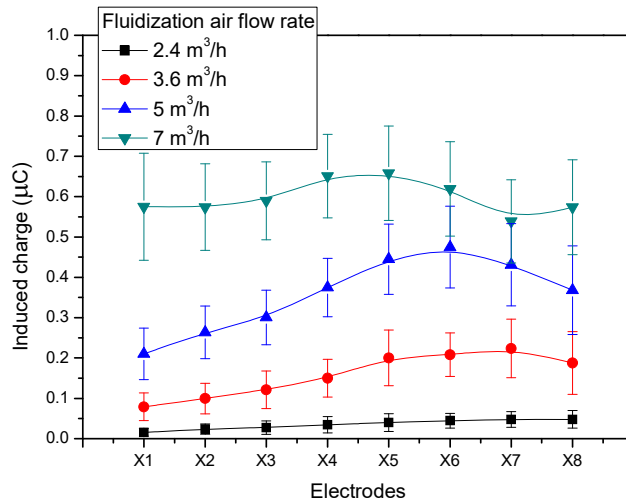
B. Splash region

In the fluidized bed, with the movement of air bubble, solid particles move upwards and bed height expands. In order to conduct the experiments in the splash region, sand particles were initially added, forming a static bed height of 200 mm. Since the wire-mesh sensors are installed at the position of 250 mm above the distributor, the electrostatic signals from the sensors reflect the charge distribution in the splash region. The flow dynamics of the splash region is dominated by the bubble bursting at the bed surface. Due to eruptions of the bubbles, the solids particles are splashed upwards at first and then dropped downwards due to gravity. As a result, the flow behavior in this region is more complex. Induced charges on electrodes X1 and X4 for fluidization air flow rates of 2.4 m³/h and 7 m³/h in the splash region are shown in Figure 13. In comparison with the results from Figure 10, the induced charge on each electrode for the same air flow rate is smaller due to lower concentration of particles in this region. Figure 14 shows time averaged and corresponding standard deviations of induced charges on different electrodes for different fluidization air flow rates. Because of the highly turbulent solids flow behavior in the splash region, the standard deviation of the induced charge on each electrode during the sampling period is higher. It is found that average induced charges on all electrodes increase with the fluidization air flow rate because of the higher solids concentration in the region. Additionally, the difference in the induced charge between the electrode in the center and that near the wall is not as obvious as that in the dense phase region.
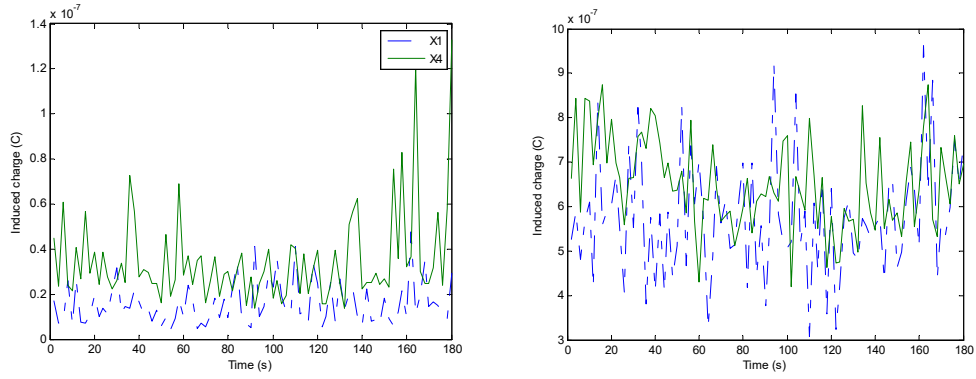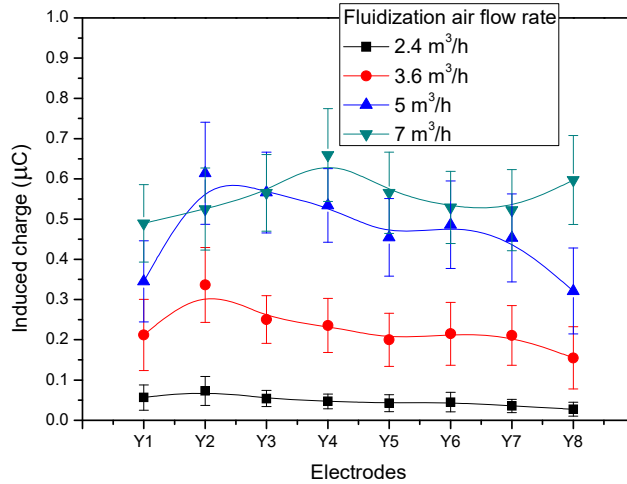
(a) Fluidization air flow rate 2.4 m³/h   (b) Fluidization air flow rate 7 m³/h

Figure 13 Induced charges on electrodes X1 and X4 in the splash region
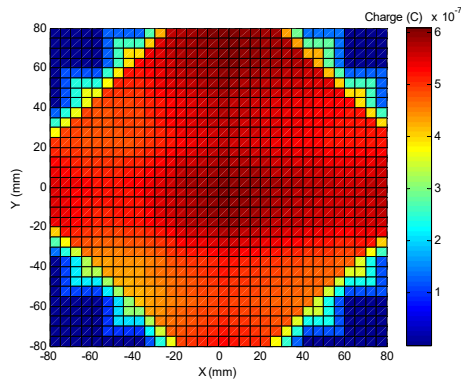

(a) Electrodes X1 to X8
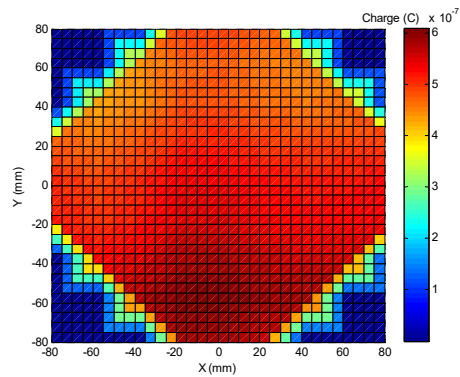

(b) Electrodes Y1 to Y8

Figure 14 Time averaged and corresponding standard deviations of induced charges on different electrodes in the splash region

Reconstructed charge distribution in the splash region for fluidization air flow rate of 7 m³/h is

21

given in Figure 15. The color bar represents the estimated quantity of the charge. Due to the

complex behavior of solid particles in this region, the charge distributions at different times are

shown. The charges in different parts of the cross section change a lot during the sampling period.

For example, the charges in the back wall region are higher at 40 second, while at 80 second, the

highest charge in the cross section changes to the front wall region and finally at 160 second, the

charges in the left wall region become higher. Average charges of the cross section for different

fluidization air flow rates are shown in Figure 16. With the increase of fluidization air flow rate,

there will be higher solids concentration in the splash region, resulting in higher average charge in

the cross section. The average charge in the cross section is calculated every two seconds and the

sampling duration is 180 seconds. Time averaged and corresponding standard deviations of the 90

average charges during the sampling period are calculated, as shown in Figure 17. Due to the

lower solids concentration in this region, the average charge of the cross section is much lower

than that of the dense phase region. In addition, the solids flow behavior becomes more turbulent

with fluidization air flow rate. As a result, the standard deviation of the average charge of the cross

section during the sampling period increases.
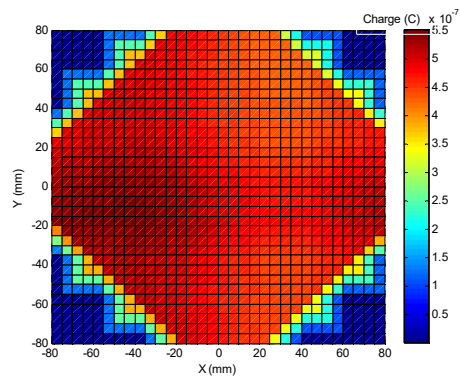

(a) at 40 second   (b) at 80 second
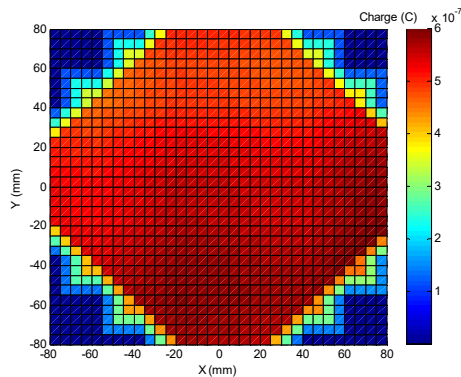
(c) at 120 second   (b) at 160 second

Figure 15 Reconstructed charge distribution in the splash region for fluidization air flow rate of 7 m³/h
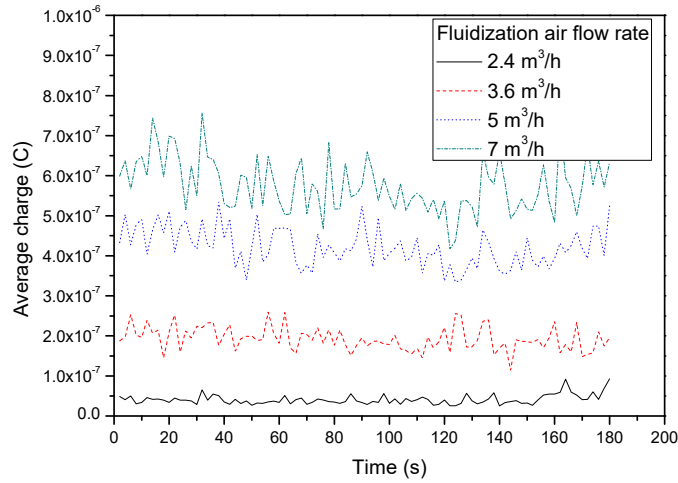

Figure 16 Average charges of the cross section for different fluidization air flow rates in the splash region
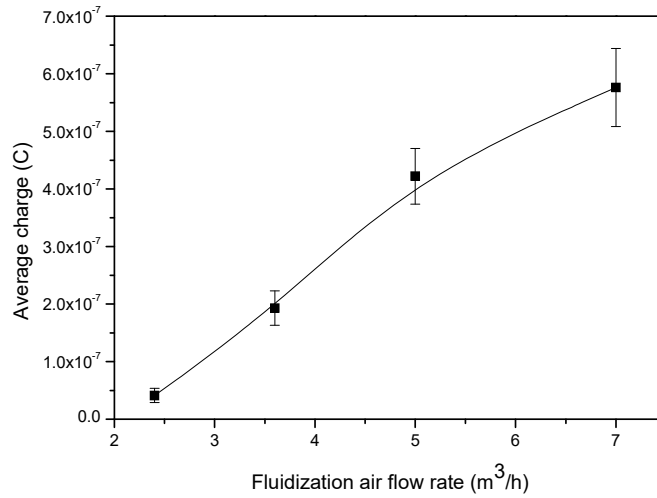

Figure 17 Time averaged and corresponding standard deviations of the average charges of the cross section

VI. CONCLUSION

In this paper, wire-mesh electrostatic sensors have been introduced to measure the charge distribution in a bubbling fluidized bed. A charge calibration process was conducted in order to establish the relationship between the induced charge on the electrode and the electrostatic signal. In the process a capacitor with adjustable charge on it acts as a charged particle. In order to verify the method of charge distribution measurement, the characteristics of the induced charges on the electrodes and the charge distribution in different parts of the bubbling fluidized bed are investigated. It has been found that, in the dense phase region, the induced charge on the electrode in the center of the cross section is higher than that in the near wall region and the charge

distribution in the cross section is relatively uniform, with the maximum relative deviation from the mean charge less than 24%. However, in the splash region, the induced charges on the electrodes and the charge distribution in the cross section are strongly influenced by the turbulent flow behavior and the charges in different parts of the bed fluctuate over time.

With the knowledge of the charge distribution in the cross section, the charging state of solid particles can be monitored and the risks of electrical discharge and even explosion in the fluidized bed are minimized. The limitation of the present method lies in the intrusiveness of the wire-mesh electrodes to the particles in the bed, which is not acceptable in certain applications. Additionally, the system output is susceptible to environmental factors such as relative humidity of the fluidization air.

REFERENCES

[1] G. Hendrickson, "Electrostatics and gas phase fluidized bed polymerization reactor wall sheeting", Chemical Engineering Science, vol. 61, pp. 1041-1064, 2006.

[2] A. Sowinski, F. Salama, P. Merhani, "New technique for electrostatic charge measurement in gas–solid fluidized beds", Journal of Electrostatics, vol. 67, pp. 568-573, 2009.

[3] A. Sowinski, L. Miller, P. Merhani, "Investigation of electrostatic charge distribution in gas–solid fluidized beds", Chemical Engineering Science, vol. 65, pp. 2771-2781, 2010.

[5] A. H. Chen, H. T. Bi and J. R. Grace, "Measurement of particle charge-to-mass ratios in a gas–solids fluidized bed by a collision probe", Powder Technology, vol. 135-136, pp. 181-191, 2003.

[6] A. H. Chen, H. T. Bi and J. R. Grace, "Effects of charge distribution around bubbles on charge induction and transfer to a ball probe in gas-solid fluidized beds", Journal of Electrostatics, vol. 58, pp. 91-115, 2003.

[7] A. H. Chen, H. T. Bi, J. R. Grace, F. K. van Willigen and J. R. van Ommen, "Measurement of charge distribution around a rising bubble in a 2-D fluidized bed", AIChE. Journal, vol. 52, pp. 174-184, 2006.

[8] A. H. Chen, H. T. Bi and J. R. Grace, "Effects of probe numbers and arrangement on the measurement of charge distributions around a rising bubble in a two-dimensional fluidized bed", Chemical engineering science, vol. 61, pp. 6499-6510, 2006.

[9] A. H. Chen, H. T. Bi and J. R. Grace, "Charge distribution around a rising bubble in a two-dimensional fluidized bed by signal reconstruction", Powder Technology, vol. 177, pp. 113-124, 2007.

[10] C. He, H. T. Bi and J. R. Grace, "Simultaneous measurements of particle charge density and

bubble properties in gas-solid fluidized beds by dual-tip electrostatic probes", Chemical engineering science, vol. 123, pp. 11-21, 2015.

[11] C. He, H. T. Bi and J. R. Grace, "A novel dual-material probe for in situ measurement of particle charge densities in gas–solid fluidized beds", Particuology, vol. 21, pp. 20-31, 2015.

[12] R. G. Green, M. F. Rahmat, K. Evans, A. Goude, M. Henry and J. A. R. Stone, "Concentration profiles of dry powders in a gravity conveyor using an electrodynamic tomography system", Measurement Science and Technology, vol. 8, pp. 192-197, 1997.

[13] M. Machida and B. Scarlett, "Process tomography system by electrostatic charge carried by particles", IEEE Sensors Journal, vol. 5, pp. 251-259, 2005.

[14] B. Zhou and J. Y. Zhang, "A novel ECT–EST combined method for gas–solids flow pattern and charge distribution visualization", Measurement Science and Technology, vol. 24, 074003, 2013.

[15] I. T. Thuku and M. F. Rahmat, "Finite-element method modeling in 4 and 16 sensors electric-charge tomography systems for particles moving in pipeline", Flow Measurement and Instrumentation, vol. 38, pp. 9-20, 2014.

[16] J. Q. Zhang and Y. Yan, "On-line continuous measurement of particle size using electrostatic sensors", Powder Technology, vol. 135-136, pp. 164-168, 2003.

[17] V. H. F. Pena and O. M. H. Rodriguez, "Applications of wire-mesh sensors in multiphase flows", Flow Measurement and Instrumentation, vol. 45, pp. 255-273, 2015.

[18] W. B. Zhang, B. B. Yang, Y. Yan and X. C. Qian, "Charge Distribution Reconstruction in a Bubbling Fluidized Bed Using a Wire-Mesh Electrostatic Sensor," Proceedings of the IEEE Instrumentation and Measurement Technology Conference, pp. 28-32, Taipei, Taiwan, 23-26 May 2016.

[19] W. B. Zhang, C. Wang and Y. L. Wang, "Parameters selection in cross-correlation based velocimetry using circular electrostatic sensors," IEEE Transactions on Instrumentation and Measurement, vol. 59, pp. 1268-1275, 2010.

[20] W. B. Zhang, Y. Yan, Y. R. Yang and J. D. Wang, "Measurement of Flow Characteristics in a Bubbling Fluidized Bed Using Electrostatic Sensor Arrays," IEEE Transactions on Instrumentation and Measurement, vol. 65, pp. 703-712, 2016.

[21] W. B. Zhang, Y. P. Cheng, C. Wang, W. Q. Yang and C. H. Wang, "Investigation on Hydrodynamics of Triple-Bed Combined Circulating Fluidized Bed Using Electrostatic Sensor and Electrical Capacitance Tomography," Industrial & Engineering Chemistry Research, vol. 52, pp. 11198-11207, 2013.

[22] P. Mehrani, H. T. Bi and J. R. Grace, "Electrostatic charge generation in gas-solid fluidized beds", Journal of Electrostatics, vol. 63, pp. 165-173, 2005.

[23] W. O. Moughrabiah, J. R. Grace and X. T. Bi, "Effects of pressure, temperature, and gas velocity on electrostatics in gas-solid fluidized beds", Industrial Engineering Chemistry Research, vol. 48, pp. 320-325, 2009.

[24] S. Matsusaka, H. Maruyama, T. Matsuyama and M. Ghadiri, "Triboelectric charging of powders-A review", Chemical Engineering Science, vol. 65, pp. 5781-5807, 2010.

[25] A-H. Park, H. Bi and J. R. Grace, "Reduction of electrostatic charges in gas solid fluidized beds," Chemical Engineering Science, vol. 57, pp. 153-162, 2002.

[26] A. Giffin and P. Mehrani, "Effect of gas relative humidity on reactor wall fouling generated due to bed electrification in gas-solid fluidized beds," Powder Technology, vol. 235, pp. 368-375, 2013.

[27] A. Wolny and W. Kazmierczak, "Triboelectrification in fluidized bed of polystyrene,"

Chemical Engineering Science, vol. 44, pp. 2607-2610, 1989.

[28] D. Kunii and O. Levenspiel, Fluidization engineering Second Edition. Oxford: Butterworth-Heinemann, 1991.